Full Paper

High Surface Area Yttrium Oxide Nanostructures Prepared through Cathodic Electro-synthesis: Development of Facile Preparation Platform and Characterization

Mustafa Aghazadeh and Ali Ahmadi*

Materials and Nuclear Research School, Nuclear Science and Technology Research Institute (NSTRI), P.O. Box 14395-834, Tehran, Iran

*Corresponding Author, Tel.: +98-21-82064289; Fax: +98-21-82064289
E-Mail: amahmadi@aeoi.org.ir

Abstract- We reported here a simple electro-synthesis procedure to synthesize an extremely high specific surface area (SSA) yttrium oxide (Y_2O_3) nanopowder. The mesoporous (pore diameter, d≈8 nm) Y_2O_3 powder was deposited by a two-step process involving the pulse cathodic electro-deposition (PC-ED) of yttrium hydroxide film from nitrate bath at 70 ^{o}C temperature followed by calcination at 600 °C in air for 3 h. The applied pulse parameters i.e. peak current density, on-time and off-time were I_p=25 mA/cm^2, t$_{on}$=1*ms* and t$_{off}$=5*ms*, respectively. The products were characterized by means of scanning electron microscopy (SEM), X-ray diffraction (XRD), differential scanning calorimetry (DSC) and Fourier transform infrared (FTIR) spectroscopy methods. The obtained data proved that the fabricated product had pure cubic Y_2O_3 crystal structure and is composed thin wall-like morphology with SAA value of 243.7 m^2/g and mean pore size of 9 nm. From these findings, the PC-ED procedure was proposed for facile fabrication of high-SSA Y_2O_3 nanopowder.

Keywords- Yttrium oxide, Surface area, Nanopowder, Heat treatment, Cathodic electro-synthesis

1. INTRODUCTION

Yttrium oxide (Y_2O_3) ceramics have been intensively investigated for different technological purposes. For decades, yttrium oxide has been an important material in the

ceramic industry including ceramic superconductors, YSZ ceramics, MOS transistors and novel light-emitting materials [1,2]. In all above motioned applications, nano-scale and high surface area of the yttrium oxide material has key determining role in its efficiency. Hence, development a facile method for fabrication of high surface area nanostructured Y_2O_3 is an interesting research area.

It was established that cathodic electro-synthesis (CES) is a facile route for the fabricating the metal oxides and hydroxides including such as cobalt oxides [3-7], nickel oxide [8-11], lanthanum oxide [12-14], manganese oxides [12-19], cobalt hydroxide [20-26], gadolinium oxide [27,28], nickel oxide [29-33], iron oxide [34-37], zirconium oxide [38,39], and yttrium oxide [40-42]. The results of these works have shown that a various nanostructures of oxides and hydroxides with morphologies such as particle, plate, wire, tube, sphere and rod could be prepared through this method. In CES method, metal oxides could be prepared by a two-step process involving the cathodic electrodeposition of the metal hydroxide precursor followed by thermal conversion of the latter into the final oxide product. Thermal conversion of the cathodically grown hydroxides is an essential step to obtain metal oxides. Physico-chemical properties of the resulting metal oxides, including morphology, composition and crystallinity are affected by conditions prevailing in the both electrodeposition and heat treatment processes. Our previous works on the CES fabrication of Y_2O_3 have shown that fine particle-, sphere-, flaky- and brain-like nanostructures of yttrium oxide are easily achievable by cathodic electro-synthesis from additive-free nitrate/chloride salts [41-45]. Although the fabricated structures in References [42-45] had fine structures at nanoscale but their surface areas were not very high. In the present work, we tuned CES parameters for preparation of high specific surface area (SSA) crystalline cubic yttrium oxide nanopowder and found that the porous Y_2O_3 powder with high surface area of about 244 m^2/g could be prepared by a two-step method involving cathodic electrodeposition of $Y(OH)_3$ films from chloride medium at a pulse CES condition and bath temperature of 70 ^{o}C. and then thermal treatment of hydroxide precursor at 600 ^{o}C for 3h. The prepared products were analyzed by various techniques of XRD, SEM, BET, DSC-TGA and FT-IR.

2. EXPERIMENTAL PROCEDURE

2.1. Materials

Yttrium nitrate nonahydrate ($Fe(NO_3)_3 . 9H_2O$, 99.9%), was purchased from Sigma Aldrich. All materials were used as received, without any purification.

2.2. Electrosynthesis of hydroxide precursor

The cathodic electrosynthesis (CE) platform previously reported for the fabrication of magnetite nanoparticles (MNPs) [46-48], was here used for the electro-synthesis of yttrium

hydroxide thin film. A schematic view of the preparation route is provided in Fig. 1. The electrosynthesis set-up was composed of a (316 L, 5 cm×5 cm×0.5 mm) steel cathode centered between two parallel graphite anodes, as shown in Fig. 1. The electrolyte solution was prepared by dissolving 1.9 g yttrium nitrate in 1 liter aqueous solution. The electrodeposition runs were conducted on an electrochemical workstation system (Potentiostat/Galvanostat, Model: NCF-PGS 2012, Iran)with applying pulse current conditions. The peak current density, on-time and off-time were selected to be 25 mA/cm^2, 1 ms and 5 ms, respectively. The deposition time and bath temperature were 60 min and 70 ^{o}C, respectively.
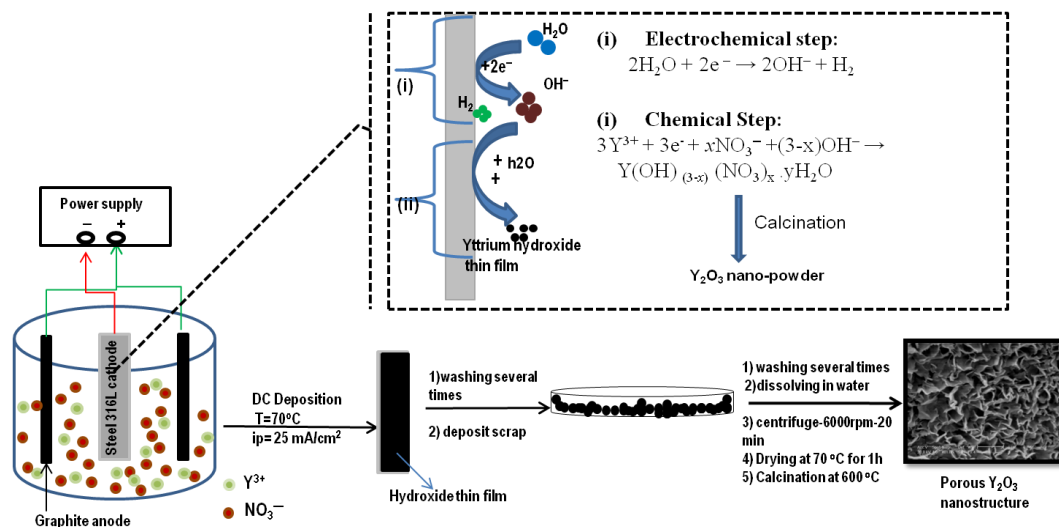

Fig. 1. Schematic graph of the cathodic electrodeposition of yttrium hydroxide and its converting to oxide product the inset presents (i) electrochemical and (ii) chemical steps of deposition procedure

After each CES experiment, the cathode was brought out from solution and rinsed several times with deionized H$_2$O. Then, the deposited black film was scraped from the steel and subjected to separation and purification steps, as noted in Fig. 1; (a) the obtained wet powder was dispersed in deionized water and centrifuged at 6000 rpm for 20 min to remove of free anions (i.e. nitrate ions), as noted in Fig. 1, (b) the deposit was then separated from water solution and dried at 70 ^{o}C for 1h, and (c) the resulting black dry powder was named hydroxide precursor, and used for calcination step.

2.3. Heat treatment step

The prepared hydroxide precursor was subjected to the calcination process in high temperature furnace. The calcination atmosphere, heating rate were dry air and 5 ^{o}C

respectively. The obtained dry powder after calcination was named as final product i.e. Y_2O_3 sample. The conversion steps of electrodeposited yttrium hydroxide into oxide were determined through differential scanning and thermogravimetric analysis.

2.4. Characterization analyses

The SEM images of the prepared powder were provided through emission scanning electron microscopy (SEM, LEO 1455VP with accelerating voltage of 30 kV). The crystal structure of the prepared powder was determined by X-ray diffraction (XRD, Phillips PW-1800) using a Cu Kα radiation. Thermal decomposition behavior of the as-prepared yttrium hydroxide powder was investigated in air using differential scanning calorimetry and thermogravimetric methods, (DSC-TGA, STA 1500) at a heating rate of 5 ^{o}C min^{-1}. FT-IR spectra were obtained by means of a Bruker Vector 22 FT-IR spectrometer. The specific surface and pore size of the final oxide product was determined through measuring N2 adsorption-desorption isotherms at 77 K with a Quanta-chrome NOVA-2200e system.

3. RESULTS AND DISCUSSION

3.1. Hydroxide formation mechanism

The cathodic deposition of metal hydroxides involves two steps; electrochemical and chemical steps. Measuring the potential values during the deposition process (−1.25 V *vs.* Ag/AgCl) revealed that the water reduction has the major role in the electrochemical step at the applied conditions, as shown in Fig. 1 as step (i).
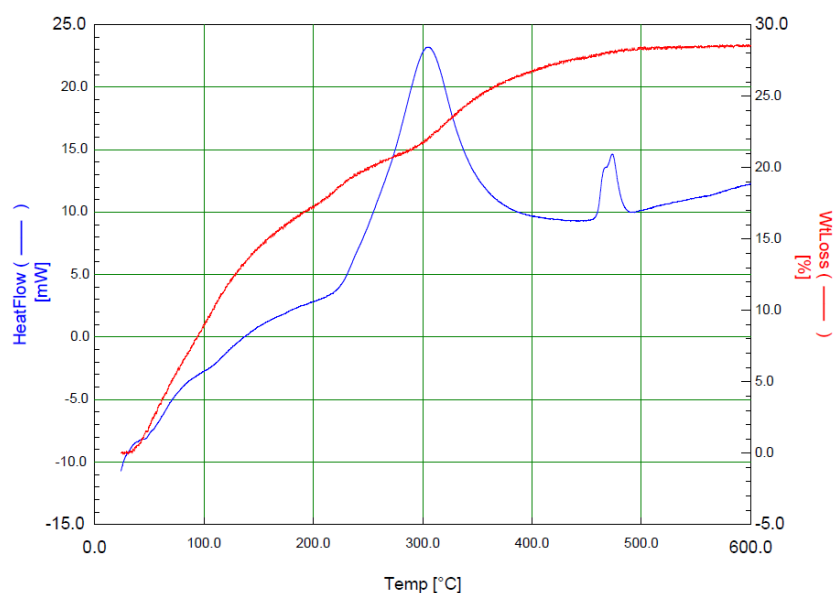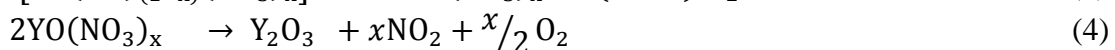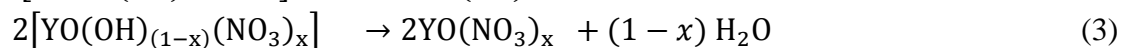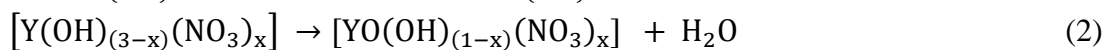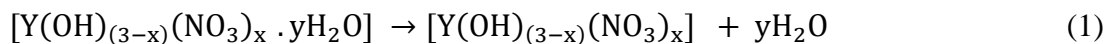

Fig. 2. DSC-TG analysis of the electro-synthesized hydroxide precursor

The string gas bubbles were experimentally observed on the cathode surface confirming the base electrogeneration via water reduction. After base generation, hydroxyl groups are reacted with yttrium cations to produce yttrium hydroxide, as indicated in Fig. 1 as step (ii).

3.2. Heat-treatment to obtain oxide product

The hydroxide film was scraped from the steel electrode and the obtain powder was heat treated at 600 $^{\circ}$C for 3 h (as schematically shown in Fig. 1c). The physico-chemical changes during this process were investigated by DSC-TG analysis and the results are shown in Fig. 2.

It can be observed that the three distinct endothermic peaks at the ranges of 25 $^{\circ}$C$<$T$<$150 $^{\circ}$C, 200 $^{\circ}$C$<$T$<$350 $^{\circ}$C, and 400 $^{\circ}$C$<$T$<$500 $^{\circ}$C. These peaks indicated the successive stages of physicochemical changes during the calcination of hydroxide, and can be interpreted by the following reactions [43,49,50]:

$$[Y(OH)_{(3-x)}(NO_3)_x \cdot yH_2O] \rightarrow [Y(OH)_{(3-x)}(NO_3)_x] + yH_2O \tag{1}$$

$$\left[Y(OH)_{(3-x)}(NO_3)_x\right] \rightarrow [YO(OH)_{(1-x)}(NO_3)_x] + H_2O \tag{2}$$

$$2\left[YO(OH)_{(1-x)}(NO_3)_x\right] \rightarrow 2YO(NO_3)_x + (1-x)H_2O \tag{3}$$

$$2YO(NO_3)_x \rightarrow Y_2O_3 + xNO_2 + {^x}/_2 O_2 \tag{4}$$

Total weight loss of the hydroxide precursor was 28.3 wt. %, as could be found in TG curve (Fig. 2).

3.3. Structural characterization of product

The XRD patterns of the prepared samples are presented in Fig. 3. The XRD pattern of the hydroxide sample by our PCED procedure have several indentified diffraction peaks, which are well matched with monoclinic phase of Y(OH)$_3$ (JCPDS No. 21-1447). Notably, the diffraction peaks of 002 and 004 are not related to monoclinic phase. It is worth noting that *00l* peaks are typically observed in the XRD pattern of layered rare-earth hydroxides (LRHs) with formula of $Ln_8(OH)_{20}(A^{m-})_{4/m} \cdot nH_2O$. In fact, the intensity and position of the *00l* peaks implicate the type and size of intercalated ions such as nitrate, chloride etc. in the synthesized hydroxide [45]. Hence, 002 and 004 peaks observed at 2θ=10.5° and 20.95° are indicative of the intercalated nitrate ions into the yttrium hydroxide deposit structure during the PCED process, as noted in inset of Fig. 1 as step (ii). And it is expected that the deposited yttrium hydroxide to has layered structure (as confirmed by SEM images, Fig. 5. Based on these data, the composition of [Y(OH)$_{3-x}$ .x(NO$_3$)$_3$]. yH$_2$O is expected formula for the deposited yttrium hydroxide. The XRD pattern of the calcined hydroxide i.e. oxide powder in Fig. 3b exhibited sharp peaks, which are readily indexed to a pure cubic phase of Y$_2$O$_3$ (space

group Ia3/(206 1)) with a lattice constant a=10.604 Å (JCPDS 25-1200). As a result, XRD data confirmed the fabrication of crystalline Y_2O_3 through propsed pulse CE method.
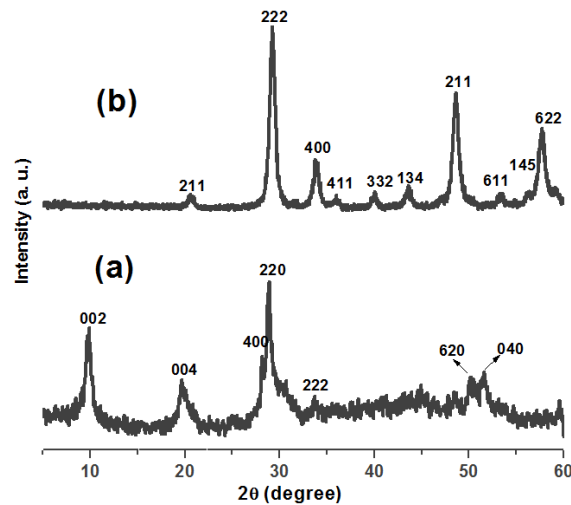

Fig. 3. XRD patterns of (a) the electrodeposited and (b) heat-treated samples

Fig. 4 shows the FTIR spectra of both electro-synthesized and calcined powders. In both of IR spectra, the bands at the wavenumber range of 3450-3500 cm^{-1} and 1640-50 cm^{-1} are originated from the stretching mode of O–H bond and bending mode water molecules attached onto the structure of samples, respectively. Also, the IR bands below 1000 cm^{-1} are related to the stretching vibrations of metal–oxygen of cubic Y_2O_3 and $Y(OH)_3$.
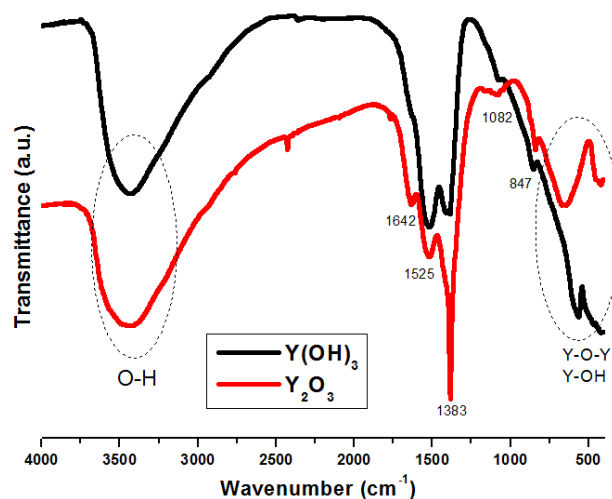

Fig. 4. FT-IR spectra of (a) the electrosynthesized yttrium hydroxide and (b) calcined oxide

The peaks at about 1525, 1430 and 1082 cm^{-1} are due to stretching modes of carbonate group, which may also originate from air [43,49]. The intense peak at 1383 cm^{-1} comes from

nitrate ions and indicative of their intercalation in the hydroxide structure [42-44]. The absence of this characteristic peaks showed their completely removal during calcination process and purity of the fabricated yttrium oxide. These data are matched with the XRD data showing the nano-crystalline Y_2O_3 powder as our product.

3.4. Morphological characterization of product

Fig. 5 shows the SEM of the fabricated Y_2O_3. From the SEM images, it is seen that the sample has wall-like morphology with a large number of cavity or pores between the walls. The observed wall is at nanoscale and uniform size and thickness (Fig. 5). It is obvious that application of thermal treatment on the as-prepared powder leads to a loss of surface uniformity of the final oxide material (Figs. 5c and d). The uniformity of Y_2O_3 porous walls is completely observable in low magnification image in Fig. 5a. This porous texture is composed of interconnected walls at nanoscale with thickness of ~50 nm and wall length of up to 500 nm. These observations indicated that the uniform porous Y_2O_3 nano-walls in large scale can be synthesized by pulse electrosynthesis. Notably, the pulse condition have major role in the uniformity of the electrodeposited product [38,41]. This regularity and uniformity in the morphology and pore could lead to large surface area of the fabricated oxide product.
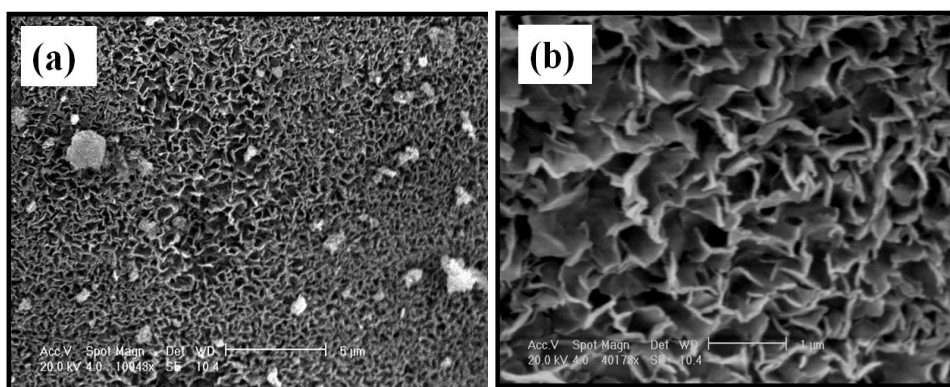

Fig. 5. SEM images of the fabricated Y_2O_3 product

Surface area and pore size distribution of the prepared oxide sample was studied through N_2 adsorption and desorption test. Fig. 6 shows the BET profile and pore size distribution curve of the yttrium oxide. N_2 desorption/adsorption isotherm and the corresponding BJH (Barret-Joyner-Halenda) pore size distribution curve of the fabricated Y_2O_3 are shown in Fig. 6. The N_2 isotherm of the fabricated Y_2O_3 has a type II form with a large type H4 hysteresis loop, indicating the presence of microporous materials according to the IUPAC classification [51]. The H_4 loop, which does not exhibit any limiting adsorption, is indicating the high ratio of porous the fabricated Y_2O_3 walls [51]. The H4 loop is also observed with aggregates of Y_2O_3 walls giving rise to slit-shaped pores. The prepared product exhibited two type of pores

i.e. microporous and mesoporous with mean diameters of 3 nm and 9 nm, respectively. Also, the fabricated Y_2O_3 have specific surface area as high as 243.6 m^2/g, which is very larger than those reported for Y_2O_3 until now [42-45, 49-50].
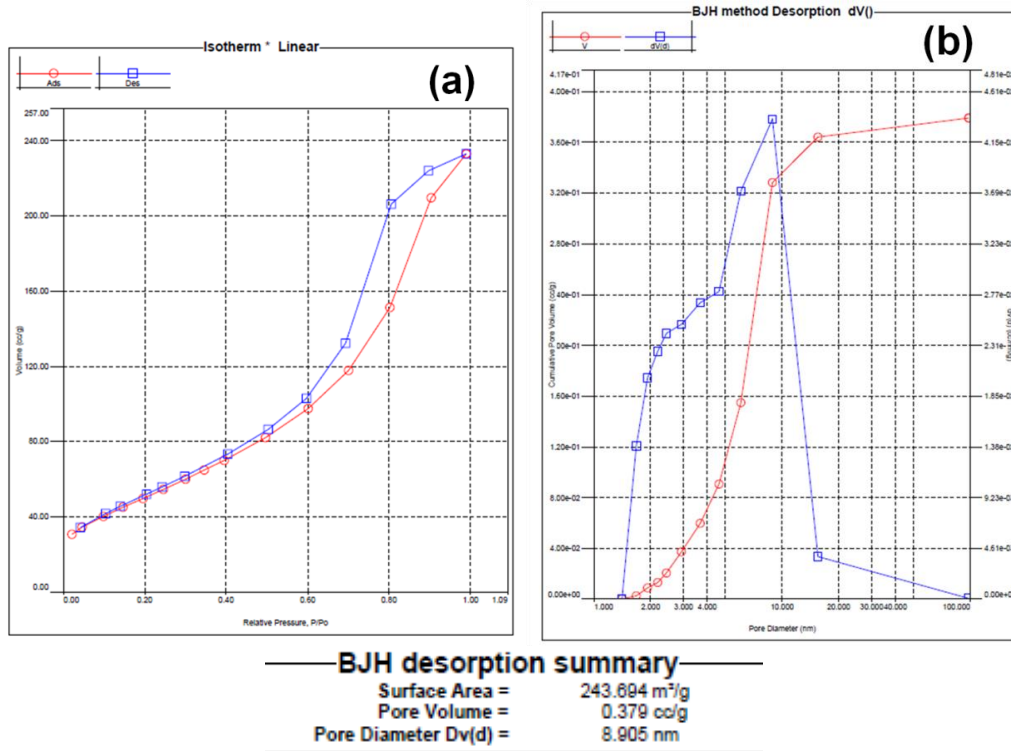

Fig. 6. (a) BET profile and (b) pore size distribution of the prepared oxide product

4. CONCLUSION

In summary, we developed a pulse electrosynthesis procedure for preparation of high surface are yttrium oxide nanopowder. The cubic phase, pure structure, wall-like morphology, mesoporous and high surface area of the fabricated Y_2O_3 powder were confirmed through XRD, IR, SEM and BET techniques. This method can be proposed for preparation of high surface area of other metal oxides.

REFERENCES

[1]   A. Sidorowicz , A. Wajler, H. Węglarz, M. Nakielska, K. Orliński, R. Diduszko, and A. Olszyna, J. Alloys Compd. 709 (2017) 293.

[2]   Y. P. Fu, J. Mater. Sci. 42 (2007) 5165.

[3]   P. Razmjoo, B. Sabour, S. Dalvand, M. Aghazadeh, and M. R. Ganjali, J. Electrochem. Soc. 161 (2014) D293.

[4] M. Aghazadeh, R. Ahmadi, D. Gharailou, M. R. Ganjali, and P. Norouzi, J. Mater. Sci. Mater. Electron. 27 (2016) 8623.

[5] M. Aghazadeh, J. Appl. Electrochem. 42 (2012) 89.

[6] M. Aghazadeh, A. Rashidy, and P. Norouzi, Int. J. Electrochem. Sci. 11 (2016) 11016.

[7] M. Aghazadeh, M. Hosseinifard, B. Sabour, and S. Dalvand, Appl. Surf. Sci. 287 (2013) 187.

[8] M. Aghazadeh, A. Rashidi, and M. R. Ganjali, Int. J. Electrochem. Sci. 11 (2016) 11002.

[9] M. Aghazadeh, M. G. Maragheh, M. R. Ganjali, and P. Norouzi, Inorg. Nano-Metal Chem. 27 (2017) 1085.

[10] A. Barani, M. Aghazadeh, M. R. Ganjali, B. Sabour, A. A. M. Barmi, and S. Dalvand, Mater. Sci. Semiconduct. Process. 23 (2014) 85.

[11] H. M. Shiri, and M. Aghazadeh, J. Electrochem. Soc. 159 (2012) E132.

[12] M. Aghazadeh, B. Arhami, A. A. M. Barmi, M. Hosseinifard, and D. Gharailou, Mater. Lett. 115 (2014) 68.

[13] F. Khosrow-pour, M. Aghazadeh, S. Dalvand, and B. Sabour, Mater. Lett. 104 (2013) 61.

[14] F. Khosrow-pour, M. Aghazadeh, and B. Arhami, J. Electrochem. Soc. 160 (2013) D150.

[15] M. Aghazadeh, A. Bahrami-Samani, D. Gharailou, M. G. Maragheh, and M. R. Ganjali, J. Mater. Sci. 27 (2016) 11192.

[16] M. Aghazadeh, M. R. Ganjali, and P. Norouzi, J. Mater. Sci. 27 (2016) 7707.

[17] M. Aghazadeh, M. R. Ganjali, and P. Norouzi, Mater. Res. Express 3 (2016) 055013.

[18] M. Aghazadeh, M. G. Maragheh, M. R. Ganjali, P. Norouzi, and F. Faridbod, Appl. Surf. Sci. 364 (2016) 141.

[19] M. Aghazadeh, M. R. Ganjali, and P. Noruzi, Thin Solid Films 634 (2017) 24.

[20] M. Aghazadeh, A. A. Malek Barmi, D. Gharailou, M. H. Peyrovi, B. Sabour, and F. Najafi, Appl. Surf. Sci. 283 (2013) 871.

[21] A. A. M. Barmi, M. Aghazadeh, B. Arhami, H. M. Shiri, A. A. Fazl, and E. Jangju, Chem. Phys. Lett. 541 (2012) 65.

[22] M. Aghazadeh, and S. Dalvand, J. Electrochem. Soc. 161 (2014) D18.

[23] M. Aghazadeh, S. Dalvand, and M. Hosseinifard, Ceram. Int. 40 (2014) 3485.

[24] M. Aghazadeh, H. Mohammad Shiri, and A. A. Malek Barmi, Appl. Surf. Sci. 273 (2013) 237-242.

[25] J. T. Mehrabad, M. Aghazadeh, M. G. Maragheh, and M. R. Ganjali, Mater. Lett. 184 (2016) 223.

[26] M. Aghazadeh, and M. R. Ganjali, J. Mater. Sci.: Mater. Electron. (2017) doi: 10.1007/s10854-017-6935-1.

[27] F. Abed, M. Aghazadeh, and B. Arhami, Mater. Lett. 99 (2013) 11.

[28] M. Aghazadeh, and T. Yousefi, Mater. Lett. 73 (2012) 176.

[29] M. Aghazadeh, A. NozadGolikand, and M. Ghaemi, Int. J. Hydrogen Energy 36 (2011) 8674.

[30] J. Tizfahm, B. Safibonab, M. Aghazadeh, A. Majdabadi, B. Sabour, and S. Dalvand, Colloids Surf. A 443 (2014) 544.

[31] M. Aghazadeh, B. Sabour, M. R. Ganjali, and S. Dalvand, Appl. Surf. Sci. 313 (2014) 581.

[32] J. Tizfahm, M. Aghazadeh, M. G. Maragheh, M. R. Ganjali, and P. Norouzi, Mater. Lett. 167 (2016) 153.

[33] M. Aghazadeh, I. Karimzadeh, and M. R. Ganjali, J. Mater. Sci. Mater. Electron. (2017) doi: 10.1007/s10854.

[34] I. Karimzadeh, M. Aghazadeh, T. Doroudi, M. R. Ganjali, and P. H. Kolivand, Mater. Res. Innovations (2017) 1. doi:10.1080/14328917.2017.1323991.

[35] M. Aghazadeh, I. Karimzadeh, M. R. Ganjali, and M. Mohebi Morad, Mater. Lett. 196 (2017) 392.

[36] I. Karimzadeh, M. Aghazadeh, T. Doroudi, M. R. Ganjali, and D. Gharailou, J. Cluster Sci. 28 (2017) 1259.

[37] M. Aghazadeh, and M. Hosseinifard, Ceram. Int. 39 (2013) 4427.

[38] M. Aghazadeh, A. A. M. Barmi, and M. Hosseinifard, Mater. Lett. 73 (2012) 28.

[39] M. Aghazadeh, T. Yousefi, and M. Ghaemi, J. Rare Earths 30 (2011) 236.

[40] M. Aghazadeh, A. A. M. Barmi, H. M. Shiri, and S. Sedaghat, Ceram. Int. 39 (2013) 1045.

[41] M. Aghazadeh, M. Ghaemi, A. N. Golikand, and A. Ahmadi, Mater. Lett. 65 (2011) 2545.

[42] M. Aghazadeh, A. A. M. Barmi, and H. M. Shiri, Russ. J. Electrochem. 49 (2013) 344.

[43] M. Aghazadeh, M. Hosseinifard, M. H. Peyrovi, and B. Sabour, J. Rare Earths 31 (2013) 281.

[44] I. Karimzadeh, M. Aghazadeh, M. R. Ganjali, P. Norouzi, and T. Doroudi, Mater. Lett. 189 (2017) 290.

[45] T. Yousefi, and M. Aghazadeh, J. Nanoengin. Nanomanufact. 2 (2012) 248.

[46] I. Karimzadeh, M. Aghazadeh, M. R. Ganjali, P. Norouzi, and T. Doroudi, Mater. Lett. 189 (2017) 290.

[47] I. Karimzadeh, M. Aghazadeh, M. R. Ganjali, P. Norouzi, and S. Shirvani-Arani, Mater. Lett. 179 (2016) 5.

[48] I. Karimzadeh, M. Aghazadeh, M. R. Ganjali, and T. Dourudi, Curr. Nanosci. 13 (2017) 167.

[49] M. Hajizadeh-Oghaz, R. Shoja Razavi, M. Barekat, M. Naderi, S. Malekzadeh, and M. Rezazadeh, J. Sol-Gel Sci. Technol. 78 (2016) 682.

[50] H. X. Zhong, Y. L. Ma, X. F. Cao, X. T. Chen, and Z. L. Xue, J. Phys. Chem. C 113 (2009) 3461.

[51] M. Aghazadeh, M. Ghaemi, B. Sabour, S. Dalvand, J. Solid State Electrochem. 18 (2013) 1569.